Check for updates

ADVANCED FUNCTIONAL MATERIALS
www.afm-journal.de

High-Detectivity UV–Visible–NIR Broadband Polymer Photodetector with Polymer Charge Blocking Layer Cross-Linked by Organic Photocrosslinker

*Hyocheol Jung, Tai Nguyen, Soyeon Kim, Jae Woong Lee, Hyeonggeun Yu, Junsung Park, Chanwoo Lim, Jihoon Lee, and Do Young Kim**

Ultraviolet (UV), visible, and near-infrared (NIR) broadband organic photodetectors are fabricated by sequential solution-based thin film coatings of a polymer electron blocking layer (EBL) and a polymer photoactive layer. To avoid damage to a preceding polymer EBL during a subsequent solution-based film coating of a polymer photoactive layer due to lack of solvent orthogonality, 2-(((4-azido-2,3,5,6-tetrafluorobenzoyl)oxy)methyl)—2-ethylpropane-1,3-diyl bis(4-azido-2,3,5,6-tetrafluorobenzoate) (FPA-3F) is used as a novel organic cross-linking agent activated by UV irradiation with a wavelength of 254 nm. Solution-processed poly[N,N′-bis(4-butylphenyl)-N,N′-bis(phenyl)-benzidine] (poly-TPD) films, which are cross-linked with a FPA-3F photocrosslinker, are used for a preceding polymer EBL. A ternary blend film composed of PTB7-Th, COi8DFIC, and $PC_{71}BM$ is used as a NIR-sensitive organic photoactive layer with strong photosensitivity in multispectral (UV–visible–NIR) wavelengths of 300–1,050 nm. Poly-TPD films are successfully cross-linked even with a very small amount of 1 wt% FPA-3F. Small amounts of FPA-3F have little detrimental effect on the electrical and optoelectronic properties of the cross-linked poly-TPD EBL. Finally, organic NIR photodetectors with a poly-TPD EBL cross-linked by the small addition of FPA-3F (1 wt%) show the detectivity values higher than 1×10^{12} Jones for the entire UV–visible–NIR wavelengths from 300 nm to 1050 nm, and the maximum detectivity values of 1.41×10^{13} Jones and 8.90×10^{12} Jones at the NIR wavelengths of 900 and 1000 nm, respectively.

1. Introduction

Visible and near-infrared (NIR) broadband photodetectors are widely used in optical communications, imaging, security, ranging, and consumer electronics.[1–4] Solution-processed photodetectors using organic, inorganic, and hybrid materials have been developed for low-cost visible and NIR sensing applications in the past decades.[5–8] Organic photodetectors with a low-bandgap polymer-based photoactive layer are also very attractive for solution-processed low-cost visible and NIR sensing applications due to their intrinsic advantages such as excellent photosensitivity, bandgap tunability, and solution-processability.[9–12] Recently, ternary blend polymer solar cells have been reported with three absorption-complementary materials composed of PTB7-Th as a donor, $PC_{71}BM$ as a fullerene acceptor, and COi8DFIC as a non-fullerene acceptor for further enhancing coverage of solar spectrum. These ternary blend polymer solar cells showed to extend their NIR absorption range to 1050 nm making them a possible alternative to silicon (Si) for broadband

H. Jung, T. Nguyen, D. Y. Kim
School of Materials Science and Engineering
Oklahoma State University
Tulsa, Oklahoma 74106, USA
E-mail: doyoung.kim@okstate.edu
H. Jung
Center for Specialty Chemicals
Division of Specialty and Bio-Based Chemicals Technology
Korea Research Institute of Chemical Technology (KRICT)
Ulsan 44412, Republic of Korea
S. Kim, J. Lee
Department of IT·Energy Convergence (BK21 FOUR)
Korea National University of Transportation
Chungju 27469, Republic of Korea
The ORCID identification number(s) for the author(s) of this article can be found under https://doi.org/10.1002/adfm.202403094
J. W. Lee
Advanced Process and Materials R&BD Group
Korea Institute of Industrial Technology
Incheon 21999, Republic of Korea
H. Yu, J. Park, C. Lim
Advanced Photovoltaics Research Center
Korea Institute of Science and Technology
Seoul 02792, Republic of Korea
H. Yu
Nanoscience and Technology
KIST School
University of Science and Technology
Seoul 02792, Republic of Korea
J. Lee
Department of Polymer Science and Engineering
Korea National University of Transportation
Chungju 27469, Republic of Korea

DOI: 10.1002/adfm.202403094

 © 2024 Wiley-VCH GmbH

photodetectors with visible as well as NIR detection capabilities.[13,14] While organic NIR photodetectors with ternary blended polymer photoactive layers were first reported with a broadband photosensitivity from 400 to 1050 nm, they showed a limited detectivity of 3×10^{11} Jones at 1000 nm due to their high dark currents.[15] The low detectivity of the early ternary blend polymer NIR photodetector was not very competitive with existing Si-based NIR photodetectors, which had a detectivity over 1×10^{13} Jones at 1000 nm. Organic NIR photodetectors with ternary blended polymer photoactive layers were very recently reported with over 1×10^{13} Jones in a broadband wavelength range (330–1050 nm).[16]

In photodetectors, a high dark current increases overall noise currents and thus decreases the detectivity, which is the most important figure of merit of the photodetectors.[17–19] However, the low-bandgap nature of NIR-sensitive polymer semiconductors such as COi8DFIC would cause large levels of electron and hole injection under reverse bias conditions from anode and cathode, respectively, thus leading to high dark current.[20–23] To mitigate the issue of charge injection from electrodes, therefore, it is important to have an electron blocking layer (EBL) and a hole blocking layer (HBL) inserted between the electrodes and the ternary blended polymer photoactive layer. Wide-bandgap organic small molecules with a relatively deep highest occupied molecular orbital (HOMO) level or a relatively shallow lowest unoccupied molecular orbital (LUMO) level have been successfully used as the HBL or the EBL on the top of the solution-processed polymer photoactive layer, respectively because organic molecular HBLs or EBLs have been easily deposited by vacuum thermal evaporation (VTE) process on the top of the solution-processed polymer photoactive layer without damaging the underlying polymer film.[24–27] However, it is challenging to use organic materials as underlying organic EBL or HBL films under the solution-processed polymer-based photoactive layer because the underlying organic EBL or HBL films are easily damaged by subsequent solution-based film coatings of the polymer photoactive layer due to lack of solvent orthogonality. While there have been several reports on organic photodetectors using poly(3,4-ethylenedioxythiophene):poly(styrene sulfonate) (PEDOT:PSS) as an EBL[28–30] where PEDOT:PSS needs polar solvents unlike other organic materials requiring nonpolar solvents, PEDOT:PSS does not sufficiently suppress the electron injection from the anode making it an ineffective EBL due to the deep LUMO level of −3.2 eV, thus resulting in high dark current and low specific detectivity as shown in Figure S1 (Supporting Information). In addition, the chemical instability of PEDOT:PSS due to its reaction with an indium tin oxide (ITO) anode can degrade the device performance.[31,32] Therefore, alternative solution-based organic materials for an EBL are needed. To overcome this solvent orthogonality limitation in sequential polymer film coating process, polymer cross-linking processes using organic cross-linking agents have been explored in a variety of organic electronic applications.[33–36] Fluorophenyl azide (FPA)-based organic cross-linking agents have recently been introduced in polymeric gate dielectrics for solution-processed organic field-effect transistors.[37,38] However, there have been no reports yet on the use of 2-(((4-azido-2,3,5,6-tetrafluorobenzoyl)oxy)methyl)−2-ethylpropane-1,3-diyl bis(4-azido-2,3,5,6-tetrafluorobenzoate) (FPA-3F) in the charge transport layer.

In this work, FPA-3F is used as an organic cross-linking agent to avoid damages to a preceding polymer EBL during a subsequent coating of a polymer-based photoactive layer. Solution-processed poly[N,N′-bis(4-butylphenyl)-N,N′-bis(phenyl)-benzidine] (poly-TPD) films, which are cross-linked with a FPA-3F organic photocrosslinker, are used for a preceding EBL in our organic NIR photodetector structure. Compared to both reference devices with a PEDOT:PSS EBL and a photocrosslinker-free poly-TPD, the ternary blend polymer photodetectors with a cross-linked poly-TPD EBL showed a significant reduction (more than two orders of magnitude) in the dark current, thus resulting in more than one order of magnitude enhancement in the detectivity. Using three absorption-complementary materials of PTB7-Th, $PC_{71}BM$, and COi8DFIC as a ternary blend polymer photosensitizer, we have successfully fabricated the broadband polymer photodetectors with multispectral sensitivity covering UV–visible–NIR wavelength from 300 to 1050 nm. The cross-linked poly-TPD EBL devices show high detectivity of 1.4×10^{13} Jones at 900 nm and 8.9×10^{12} Jones at 1000 nm due to significantly low dark current (1.51×10^{-6} mA cm^{-2} at −0.1 V).

2. Results and Discussion

To promote the cross-linking process of an underlying polymer EBL in the polymer photodetector, FPA-3F as an organic photocrosslinker is successfully designed and synthesized. The synthetic routes and the analysis data of FPA-3F are explained in the experimental section. Solution-processed poly-TPD films are used as an underlying polymer EBL of the polymer photodetector due to its appropriate energy band alignment with the ternary blend polymer photoactive layer. **Figure 1** shows the cross-linking mechanism of poly-TPD with FPA-3F. Three azide groups of FPA-3F organic photocrosslinker create three singlet nitrene groups under deep ultraviolet (UV) irradiation of 254 nm wavelength. The singlet nitrene groups of UV-activated FPA-3F are linked with alkyl groups of poly-TPD through an alkyl C—H insertion reaction.

To evaluate the cross-linking reaction of FPA-3F as an organic photocrosslinker, four UV-irradiated poly-TPD films without FPA-3F (0 wt%) and with FPA-3F of 0.5, 1, and 3 wt% are prepared together with a reference poly-TPD film without FPA-3F and without UV irradiation. Poly-TPD precursor solutions without FPA-3F (0 wt%) or with FPA-3F (0.5, 1, and 3 wt%) are first spin-coated and annealed at 80 °C. The spin-coated poly-TPD films without FPA-3F (0 wt%) and with FPA-3F (0.5, 1, and 3 wt%) are then irradiated by UV light (254 nm wavelength) with an exposure dose of 50 mJ cm^{-2} under blowing nitrogen gas condition except a reference poly-TPD film without FPA-3F. Optical absorption spectra of poly-TPD films are measured before and after solvent washing as shown in **Figure 2**.

Chlorobenzene (CB) is used as a washing solvent because CB is the solvent for the precursor solution of the ternary blend polymer photoactive layer. Before solvent washing, all poly-TPD films show strong optical absorption at UV wavelengths below 420 nm corresponding to the optical bandgap (2.9 eV) of poly-TPD.[39–41] For the reference poly-TPD film without FPA-3F

© 2024 Wiley-VCH GmbH

16163028, 0, Downloaded from https://onlinelibrary.wiley.com/doi/10.1002/adfm.202403094 by Oklahoma State University, Wiley Online Library on [29/08/2024]. See the Terms and Conditions (https://onlinelibrary.wiley.com/terms-and-conditions) on Wiley Online Library for rules of use; OA articles are governed by the applicable Creative Commons License

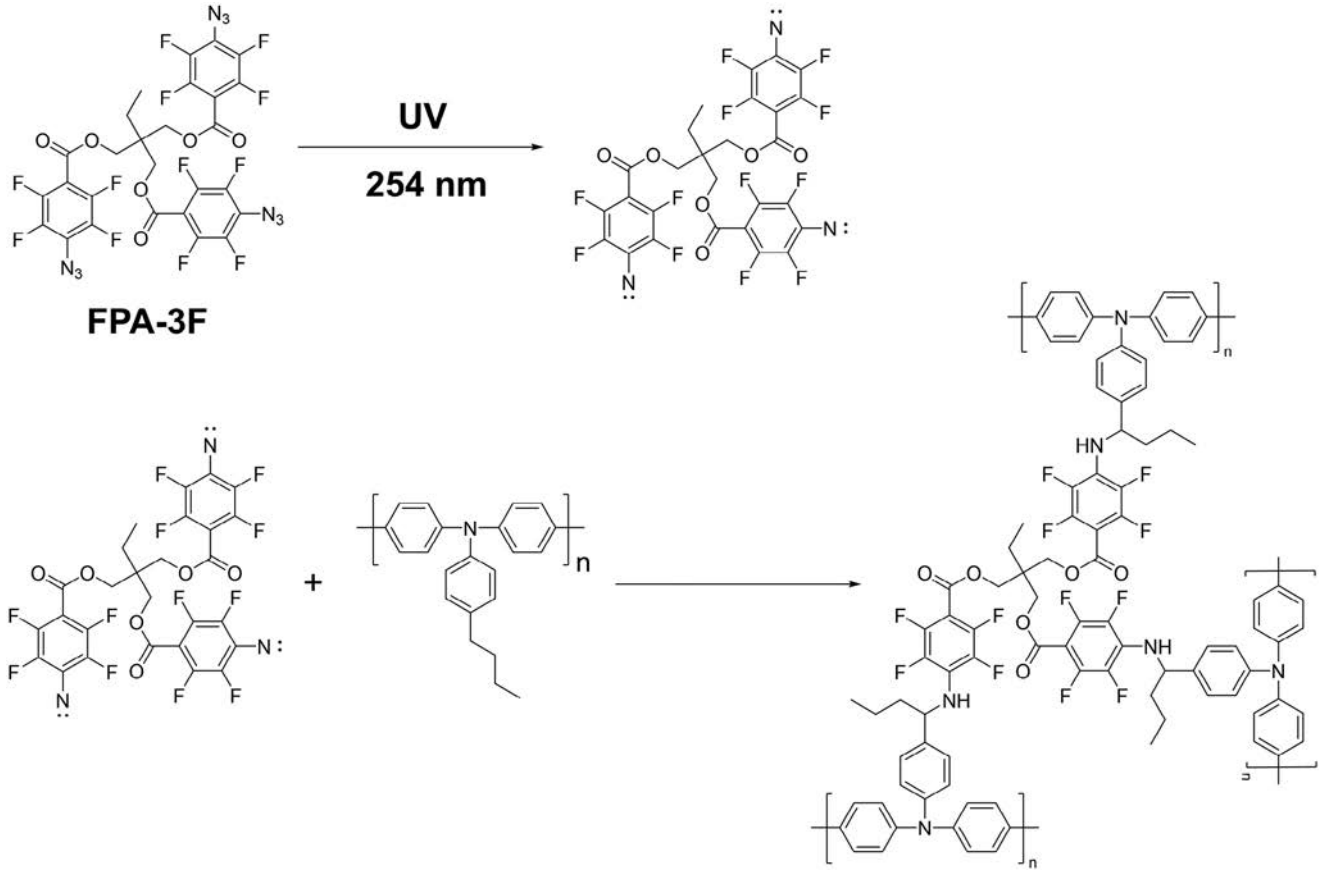

Figure 1. Cross-linking mechanism of poly-TPD with FPA-3F.

photocrosslinker and without UV irradiation, the strong UV absorption below 420 nm almost disappears after solvent washing as shown in Figure 2a, thus indicating that the poly-TPD film is almost washed away by CB as expected. With UV irradiation of a poly-TPD film without FPA-3F, the UV absorption below 420 nm does not completely disappear after solvent washing but is significantly reduced to about 15% as shown in Figure 2b, thus indicating that the poly-TPD film is still significantly washed away by CB despite UV irradiation. For the UV-irradiated poly-TPD film with FPA-3F of 0.5 wt%, the poly-TPD films after solvent washing still show UV absorption of about 40% of the original poly-TPD film before solvent washing as shown in Figure 2c, thus indicating that the poly-TPD films of about 40% remain after solvent washing. For the UV-irradiated poly-TPD film with FPA-3F of 1 and 3 wt%, the poly-TPD films after solvent washing still show UV absorption of more than 90% of the original poly-TPD film before solvent washing as shown in Figure 2d,e, thus indicating that the poly-TPD films of more than 90% remain after solvent washing. This result clearly shows that the poly-TPD films containing a small amount of FPA-3F photocrosslinkers are successfully cross-linked by UV irradiation. Most of the reported FPA-based organic photocrosslinkers have two azide groups and thus require large amounts (up to 12 wt%) of photocrosslinkers for the polymeric cross-linking processes.[37,42–48] The cross-linking capability of our FPA-3F in poly-TPD films compared to the reported FPA-2F is also evaluated with the same amount (1 wt%) and the same UV intensity (50 mJ cm^{-2}) as shown in Figure S2 (Supporting Information). While a poly-TPD film with FPA-3F after solvent washing still shows UV absorption of more than 90% of the original poly-TPD film before solvent washing, a poly-TPD film with FPA-2F after solvent washing shows only UV absorption of about 45% of the original poly-TPD film before solvent washing. These results clearly indicate that FPA-3F is a better cross-linking additive compared to FPA-2F. A large amount of photocrosslinkers causes deterioration of the electrical and optoelectronic properties of the photocrosslinked polymer films.[49] Since the FPA-3F organic photocrosslinker having three azide groups successfully cross-links the poly-TPD films even at a very small amount of 1 wt%, it is expected that the electrical and optoelectronic properties of the poly-TPD films are not severely deteriorated.

To evaluate the cross-linked poly-TPD films as an EBL for organic NIR photodetectors, photodetectors are fabricated with a ternary blend polymer photosensitizing layer containing three absorption-complementary materials of PTB7-Th, $PC_{71}BM$, and COi8DFIC. The chemical structures of PTB7-Th, $PC_{71}BM$, and COi8DFIC are shown in Figure S3 (Supporting Information). 2,9-Dimethyl-4,7-diphenyl1,10-phenanthroline (BCP) is used as HBL. The device structure is ITO/poly-TPD + x wt% FPA-3F (40 nm)/PTB7-Th:COi8DFIC:$PC_{71}BM$ (120 nm)/BCP (10 nm)/Ag(100 nm) as shown in **Figure 3a** and the corresponding energy band diagram is shown in Figure 3b. The bandgap of

© 2024 Wiley-VCH GmbH

16163028, 0, Downloaded from https://onlinelibrary.wiley.com/doi/10.1002/adfm.202403094 by Oklahoma State University, Wiley Online Library on [29/08/2024]. See the Terms and Conditions (https://onlinelibrary.wiley.com/terms-and-conditions) on Wiley Online Library for rules of use; OA articles are governed by the applicable Creative Commons License

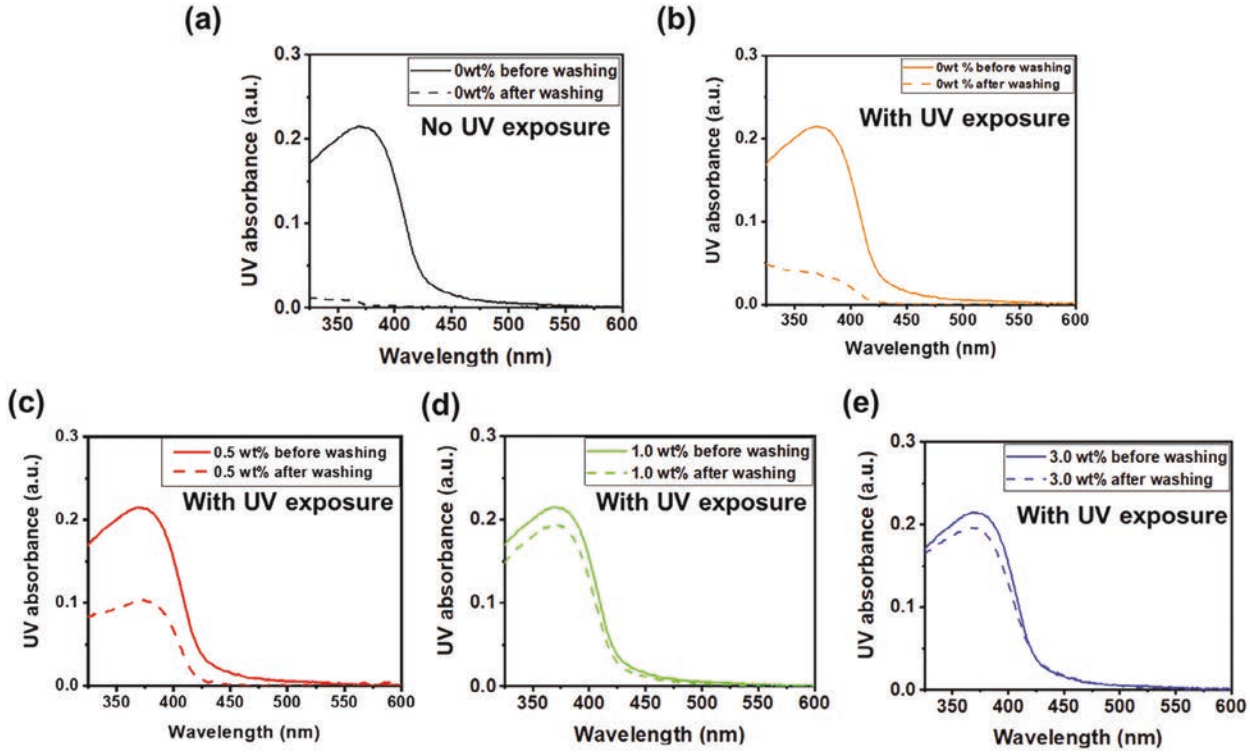

Figure 2. UV–visible absorption spectra of poly-TPD films before and after solvent washing a) without FPA-3F (0 wt%) and without UV exposure (254 nm), b) without FPA-3F (0 wt%) and with UV exposure (254 nm, 50 mJ cm^{-2}), c) with FPA-3F (0.5 wt%) and with UV exposure (254 nm, 50 mJ cm^{-2}), d) with FPA-3F (1.0 wt%) and with UV exposure (254 nm, 50 mJ cm^{-2}), and e) with FPA-3F (3.0 wt%) and with UV exposure (254 nm, 50 mJ cm^{-2}).

poly-TPD films with different FPA-3F wt% is measured by Tauc plot and provided in Figure S14 (Supporting Information). As shown in Figure S14 (Supporting Information), the bandgap is more or less the same regardless of the wt%. Figure 3c shows the current–voltage (*J*–*V*) characteristics of organic NIR photodetectors using poly-TPD EBLs cross-linked with different amounts of FPA-3F (0, 0.5, 1, and 3 wt%) in the dark and upon NIR light irradiation (power density = 2.92 mW cm^{-2}, wavelength = 900 nm). The reference photodetector without organic photocrosslinker (FPA-3F of 0 wt%) exhibits a very high dark current density of 1.36×10^{-4} mA cm^{-2} at a reverse bias of −0.1 V, thus indicating that poly TPD EBL without FPA-3F does not adequately suppress external electron injection from the ITO anode. This is because poly-TPD films without FPA-3F are hardly cross-linked and are mostly washed away in the subsequent CB-based solution-processed polymer photoactive layer coating process as shown in Figure 2a,b. However, the photodetectors using the cross-linked poly-TPD EBLs with small amounts of FPA-3F as a cross-linking agent show a significantly reduced dark current compared to the reference photodetector without FPA-3F (0 wt%). In the organic photodetectors with the cross-linked poly-TPD EBL, the dark current under a reverse bias of −0.1 V continually decreases with increasing the FPA-3F concentration and is saturated at 1.0 wt%, achieving significantly low values of 1.51×10^{-6} mA cm^{-2} at 1.0 wt% and 1.37×10^{-6} mA cm^{-2} at 3.0 wt%, respectively. This is because the well-crosslinked poly-TPD film is barely damaged by the subsequent CB-based solution-processed polymer photoactive layer coating process as shown in Figure 2d,e, and as a result, the cross-linked EBL effectively suppresses external electron injection from the ITO anode under the reverse bias. Despite significant dark current reduction due to better electron blocking effect, the photocurrents of the devices with FPA-3F are similar to that of the devices without FPA-3F. This indicates that small amounts of FPA-3F have little detrimental effect on the hole transport properties of the cross-linked poly-TPD EBL, thus extracting photogenerated holes as efficiently as devices without FPA-3F.

By the way, poly-TPD films can be cross-linked without any photocrosslinkers by UV irradiation as also shown in Figure 2b.[50,51] With a UV exposure dose of 200 mJ cm^{-2}, thus, the photo-crosslinked poly-TPD films without FPA-3F (0 wt%) cannot be distinguished from the photo-crosslinked poly-TPD films with FPA-3F (1 wt%) as shown in the optical absorption spectra in Figure S4 (Supporting Information). However, the charge transporting/blocking property of the photo-crosslinked poly-TPD films without FPA-3F (0 wt%) is quite different from that with FPA-3F (1 wt%) as shown in Figure S5 (Supporting Information). Figure S5a,b (Supporting Information) shows the dark *J*–*V* curves of organic NIR photodetectors using the photo-crosslinked poly-TPD EBLs without FPA-3F (0 wt%) and with FPA-3F (1.0 wt%), respectively. All eight organic photodetectors with the photo-crosslinked poly-TPD EBL containing FPA-3F (1.0 wt%) show uniformly low dark current densities of less than 2×10^{-6} mA cm^{-2} at a reverse bias of −0.1 V. However, the photo-crosslinked poly-TPD EBL without the addition of FPA-3F (0 wt%) has very low reproducibility as an EBL, and most devices using it show a very high dark current density

© 2024 Wiley-VCH GmbH

16163028, 0, Downloaded from https://onlinelibrary.wiley.com/doi/10.1002/adfm.202403094 by Oklahoma State University, Wiley Online Library on [29/08/2024]. See the Terms and Conditions (https://onlinelibrary.wiley.com/terms-and-conditions) on Wiley Online Library for rules of use; OA articles are governed by the applicable Creative Commons License

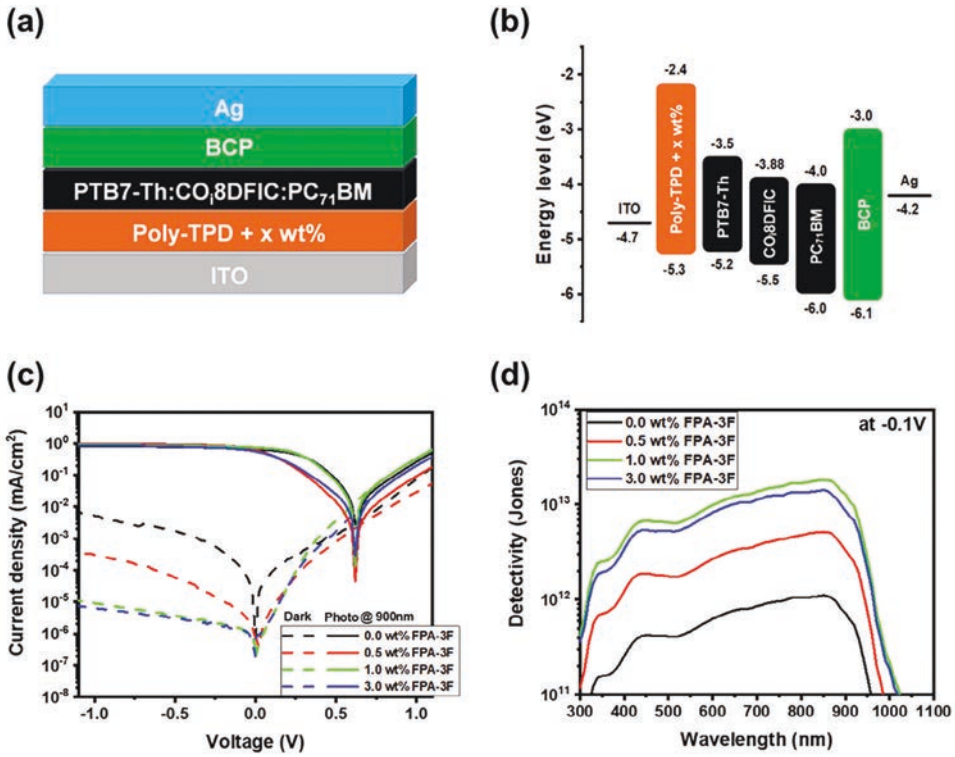

Figure 3. a) Schematic cross-sectional view of organic NIR photodetectors with poly-TPD EBLs, b) schematic energy band diagram of organic NIR photodetectors with poly-TPD EBLs, c) *J–V* characteristics of organic NIR photodetectors with poly-TPD EBLs containing various FPA-3F contents, and d) specific detectivity spectra under an applied bias of −0.1 V of organic NIR photodetectors with poly-TPD EBLs containing various FPA-3F contents.

compared to devices using FPA-3F. This indicates that in the absence of a photocrosslinker (FPA-3F), the crosslinking reaction occurs unevenly throughout the poly-TPD film, thus causing some noncrosslinked regions in the poly-TPD film. As a result, noncrosslinked regions of the poly-TPD film may be damaged in the subsequent CB-based solution-processed polymer photoactive layer coating process, and these damaged regions become electrical leakage paths that cause high dark current. Therefore, to reproducibly create cross-linked poly-TPD films with charge transporting/blocking properties applicable to electronic devices, adding a small amount of FPA-3F as a photocrosslinker is of great advantage.

The figure of merit for evaluating a photodetector performance is the specific detectivity (D*). The expression used for calculating specific detectivity is:

$$D* = \frac{(A\Delta f)^{1/2} R}{i_n} \quad (1)$$

where R is the responsivity, A is the detector area, Δf is the bandwidth, and i_n is the noise current.[52,53] Assuming that shot noise due to the dark current is the primary contribution in the total noise current of the photodetector, the specific detectivity is then given by the following equation:[54]

$$D* = \frac{R}{\sqrt{2qJ_d}} = \frac{\mathrm{EQE} \times \lambda \times q}{hc} \times \frac{1}{\sqrt{2qJ_d}} = \frac{J_{ph}}{J_{light}} \times \frac{1}{\sqrt{2qJ_d}} \quad (2)$$

where R is the responsivity, q is the electronic charge, J_{ph} is the photocurrent density, J_d is the dark current density, L_{light} is the intensity of the incident light, EQE is the external quantum efficiency, λ is the wavelength of the incident light, h is the Planck constant, and c is the speed of light. As shown in Equation (2), a high detectivity requires photodetectors with a high photocurrent (or EQE) and a low dark current. The spectral EQE values of organic NIR photodetectors using cross-linked poly-TPD EBLs with different amounts of FPA-3F (0, 0.5, 1, and 3 wt%) are measured under a reverse bias of −0.1 V as shown in Figure S6 (Supporting Information). The EQE values of the poly-TPD EBL devices with different amounts of FPA-3F (0, 0.5, 1, and 3 wt%) are similar to each other across the entire visible and near-IR wavelengths. This is in great agreement with the photocurrent results of the *J–V* characteristics (Figure 3c). Unlike similar photocurrent values, the dark current values of the photodetectors using cross-linked poly-TPD EBLs vary by several orders of magnitude depending on the FPA-3F content of the poly-TPD EBLs. As a result, the spectral detectivity values of the photodetectors with cross-linked poly-TPD EBLs are also varied by several orders of magnitude depending on the FPA-3F content of the poly-TPD EBLs and the highest detectivity value is obtained at 1.0 wt% FPA-3F as shown in Figure 3d. The organic photodetector with a cross-linked poly-TPD EBL containing FPA-3F of 1.0 wt% shows the detectivity values of 1.28×10^{13} Jones and 2.15×10^{11} Jones at NIR wavelengths of 900 and 1000 nm, respectively. These are approximately 20 times higher than that of the reference device without FPA-3F. This enhancement in detectivity is due to the lowered dark

© 2024 Wiley-VCH GmbH

16163028, 0, Downloaded from https://onlinelibrary.wiley.com/doi/10.1002/adfm.202403094 by Oklahoma State University, Wiley Online Library on [29/08/2024]. See the Terms and Conditions (https://onlinelibrary.wiley.com/terms-and-conditions) on Wiley Online Library for rules of use; OA articles are governed by the applicable Creative Commons License

Table 1. Device performances of organic NIR photodetectors with the poly-TPD containing the different amounts of FPA-3F.

The amount of FPA-3F [wt%]	Dark current [mA cm^{-2}]	Photocurrent[a,b] [mA cm^{-2}]	Responsivity [A W^{-1}]	Detectivity[a] [Jones]
0.0	1.36×10^{-4}	0.70	0.23	7.25×10^{11}
0.5	5.31×10^{-6}	0.77	0.27	3.30×10^{12}
1.0	1.51×10^{-6}	0.79	0.27	1.28×10^{13}
3.0	1.37×10^{-6}	0.66	0.18	8.61×10^{12}

[a] At −0.1 V; [b] At 900 nm.

Table 2. Device performances of organic NIR photodetector with different photoactive layer thicknesses.

The amount of FPA-3F [wt%]	Photocurrent[a] [mA cm^{-2}]	Responsivity[a] [A W^{-1}]	Detectivity[a] [Jones]	Detectivity[b] [Jones]
90	0.70	0.22	1.07×10^{13}	1.71×10^{11}
120	0.79	0.27	1.28×10^{13}	2.15×10^{11}
150	1.14	0.41	1.38×10^{13}	3.36×10^{12}
167	1.24	0.44	1.41×10^{13}	5.75×10^{12}
180	1.00	0.40	1.24×10^{13}	8.90×10^{12}
200	0.85	0.29	9.10×10^{12}	3.20×10^{12}

[a] At −0.1 V and 900 nm; [b] at −0.1 V and 1000 nm.

current with a cross-linked poly-TPD EBL assisted by the organic photocrosslinker, FPA-3F. The performance of the devices is also summarized in **Table 1**.

To further enhance the detectivity of the organic NIR photodetectors especially at a relatively longer wavelength of 1000 nm, the photoactive layer thickness is increased from 90 to 200 nm by increasing precursor solution concentration from 13.5 to 27 mg mL^{-1}. **Figure 4** shows the photoactive layer thickness dependence on the detectivity and the photocurrent of organic NIR photodetectors, especially at wavelengths of 900 and 1000 nm. While increasing the active layer thickness, the light absorption, and hence the photocurrent, is expected to be enhanced due to a thicker photoactive layer. At a wavelength of 1000 nm, the detectivity of the photodetector increases significantly from 1.71 × 10^{11} Jones to 8.90 × 10^{12} Jones with an approximately 100-fold increase in photocurrent as the photoactive layer thickness increases from 90 to 180 nm. This is in great agreement with the spectral EQE results in photodetectors with different photoactive layer thicknesses (Figure S7, Supporting Information). The strong thickness dependence at a wavelength of 1000 nm indicates that the photoactive layer has much weaker absorption at 1000 nm compared to 900 nm.[13–15] As the photoactive layer thickness further increases beyond 180 nm, photocurrent begins to reduce due to the limited charge transport properties of the organic photoactive layer, and thus the detectivity of the photodetector begins to decrease. Unlike at 1000 nm wavelength, the detectivity and photocurrent did not change significantly depending on the photoactive layer thickness at 900 nm. At a wavelength of 900 nm, the detectivity of the photodetector increases slightly from 1.07 × 10^{13} to 1.41 × 10^{13} Jones as the photoactive layer thickness increases from 90 to 167 nm. As the photoactive layer thickness further increases beyond 167 nm, the detectivity of the photodetector begins to decrease. The device performances are summarized in **Table 2** and Figure S8 (Supporting Information) shows the dark and photo *J*–*V* curves of organic NIR photodetectors with different photoactive layer thicknesses.

By measuring noise current (Figure S10, Supporting Information) as shown in Equation (1), the accurate spectral detectivity of the photodetector with the photoactive layer thickness of 167 nm is obtained as shown in **Figure 5**. The detectivity values measured using noise current are 9.2 × 10^{12} Jones at a wavelength of 900 nm and 3.98 × 10^{12} Jones at a wavelength of 1000 nm. These values are the highest among the detectivity values reported at NIR wavelengths of 900 and 1000 nm as shown in Table S1 (Supporting Information). The detectivity values obtained by the noise current are approximately 30% lower than those obtained by the dark current. The detectivity values of the organic photodetector with a cross-linked poly-TPD EBL are over 1 × 10^{12} Jones for the entire UV–visible–NIR wavelengths from 300 to 1050 nm. The spectral detectivity of the organic photodetector is also compared to that of commercially-available Si photodetector. The detectivity value of the organic photodetector with the cross-linked poly-TPD EBL is significantly enhanced by using FPA-3F as a cross-linking agent, but is still 30% lower than that of the Si photodetector in the

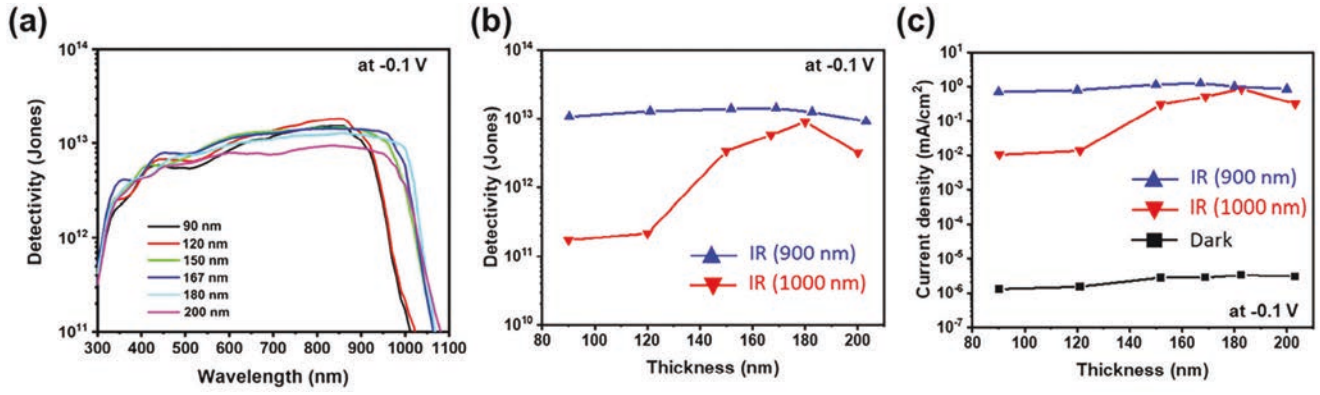

Figure 4. a) Specific detectivity spectra of the organic NIR photodetectors with different photoactive layer thicknesses under an applied reverse bias of −0.1 V, b) the photoactive layer thickness dependence on the detectivity values at wavelengths of 900 nm and 1000 nm under an applied reverse bias of −0.1 V, and c) the photoactive layer thickness dependence on the dark current and photocurrents at wavelengths of 900 nm and 1000 nm under an applied reverse bias of −0.1 V.

© 2024 Wiley-VCH GmbH

16163028, 0, Downloaded from https://onlinelibrary.wiley.com/doi/10.1002/adfm.202403094 by Oklahoma State University, Wiley Online Library on [29/08/2024]. See the Terms and Conditions (https://onlinelibrary.wiley.com/terms-and-conditions) on Wiley Online Library for rules of use; OA articles are governed by the applicable Creative Commons License

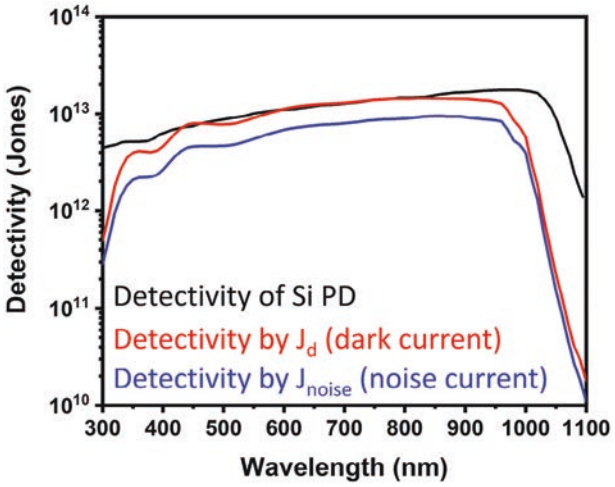

Figure 5. Spectral detectivity spectra of the organic NIR photodetectors obtained by dark current measurement (red) and noise current measurement (blue) under the applied bias of −0.1 V in comparison with commercially available Si photodetector (black).

UV-to-visible-NIR wavelengths from 350 to 950 nm. Therefore, there is still room to further improve the device performance of the organic photodetector.

It is also noted that our organic photodetector with the cross-linked poly-TPD interlayer exhibits larger built-in potential and depletion zone compared to the device with conventional PEDOT:PSS interlayer (Figure S9, Supporting Information). It implies that our cross-linked poly-TPD not only provides the electron-blocking capability but it also induces sufficient internal field for the photocarriers to be extracted from the organic active layer.

Next, we measured the dynamic response of the photodetector by AC modulating a CW diode laser with the wavelength of 940 nm and the power density of 2 mW cm^{-2} at 1 kHz. **Figure 6a** shows the rise time of 10 μS and the fall time of 19 μS, revealing sufficiently fast photo-response with the cross-linked polymer interlayer. Figure 6b shows the frequency response of the photocurrent between 10 Hz and 300 kHz. The measured −3 dB bandwidth of 46.6 kHz well matches with the extracted response times from the Figure 6a.

Figure 6c shows the linear dynamic range (LDR) measured at −0.1 V for our organic photodetector with different FPA-3F wt% and Figure 6d describes the corresponding responsivity calculated from Figure 6c. As expected from the dark/photo curves in the reverse bias region in Figure 3c, the organic photodetector with 0.5 wt% FPA-3F exhibits only 15 dB of LDR along with the LDR slope of only 0.91. On the other hand, due to the low dark current and high photo current, the organic photodetector with 1 wt% FPA-3F shows the largest LDR of 84 dB along with the slope of 0.99. Since the organic photodetector with 3 wt% FPA-3F shows the similar level of dark current in the reverse bias region as in the case of 1 wt% FPA-3F (Figure 3c), the LDR behavior in the low infrared intensity region is similar in both cases. However, the organic photodetector with 3 wt% FPA-3F reveals earlier saturation of photocurrent in the high intensity region compared to the organic photodetector with 1 wt% FPA-3F, along with the smaller LDR slope in the former case. As a result, the organic photodetector with 3 wt% FPA-3F case shows LDR of 51 dB, being smaller than the 1 wt% FPA-3F case. We further examined the LDR of 5 wt% FPA-3F case. However, the linearity of the photoresponse curve is much degraded in both low intensity and high intensity regions, compared to the 1 wt% FPA-3F case, resulting in LDR of 30 dB along with the slope of only 0.92.

To explain the difference in the LDR behaviors mainly caused by different levels of dark current, trap analysis of the poly-TPD layer with different wt% FPA-3F was performed. Figure S11 (Supporting Information) shows the relative comparison of the trap density (N_t) measured by impedance spectroscopy from ITO/poly-TPD/Al sample. The number of deep trap sites located 0.65 eV or deeper with respect to the band edge is almost three times larger in both 0.5 wt% and 5 wt% FPA-3F cases compared to the 1 wt% and 3 wt% cases. Such a trend is very similar to the dark current behavior observed in the Figure 3c where both organic photodetectors with 1 wt% and 3 wt% FPA-3F show low dark current level compared to the others. Therefore, we attribute the different dark current behavior observed in Figure 3c to electron injection through the deep trap sites in the poly-TPD in the reverse bias region.

To investigate an effect of poly-TPD film morphology on the dark current behavior, atomic force microscopy (AFM) measurement was performed on each poly-TPD film with different wt% FPA-3F. However, as observed in the AFM image (Figure S15, Supporting Information), the film with 1 wt% FPA-3F rather exhibits the highest surface roughness compared to the others, negating a scenario that any morphological impact governs the dark current behavior in Figure 3c.

The effect of different LDR is also demonstrated by 2D imaging of stripe pattern using our organic photodetector. As shown in Figure S13 (Supporting Information), our OPD with 1 wt% FPA-3F (high LDR) exhibits more drastic image contrast compared to the organic photodetector with 5 wt% FPA-3F (low LDR).

3. Conclusion

An organic NIR photodetector is successfully fabricated using a cross-linked poly-TPD EBL assisted by a novel organic photocrosslinker, FPA-3F. A very small amount of 1.0 wt% FPA-3F successfully cross-links a poly-TPD EBL. The organic photodetector using a cross-linked poly-TPD EBL with FPA-3F of 1.0 wt% shows the low dark current because the cross-linked EBL effectively suppresses external electron injection under the reverse bias. As a result, the organic photodetector using the cross-linked poly-TPD EBL shows the detectivity values higher than 1×10^{12} Jones for the entire UV–visible–NIR wavelengths from 300 to 1050 nm, and the maximum detectivity values of 1.41×10^{13} Jones and 8.90×10^{12} at the NIR wavelengths of 900 and 1000 nm, respectively.

4. Experimental Section

Synthesis of FPA-3F: To a solution of sodium azide (2 g, 31 mmol) in water (23.2 mL) and acetone (23.2 mL) in a 250 mL two-necked round-bottom flask equipped with a stirring bar and reflux condenser was added a solution of 1 (3.7 g, 5.2 mmol) in acetone (33.2 mL), and the mixture was stirred at 60 °C overnight. After the mixture was cooled to room temperature, the acetone was removed in vacuo. The reaction mixture was diluted

© 2024 Wiley-VCH GmbH

16163028, 0, Downloaded from https://onlinelibrary.wiley.com/doi/10.1002/adfm.202403094 by Oklahoma State University, Wiley Online Library on [29/08/2024]. See the Terms and Conditions (https://onlinelibrary.wiley.com/terms-and-conditions) on Wiley Online Library for rules of use; OA articles are governed by the applicable Creative Commons License

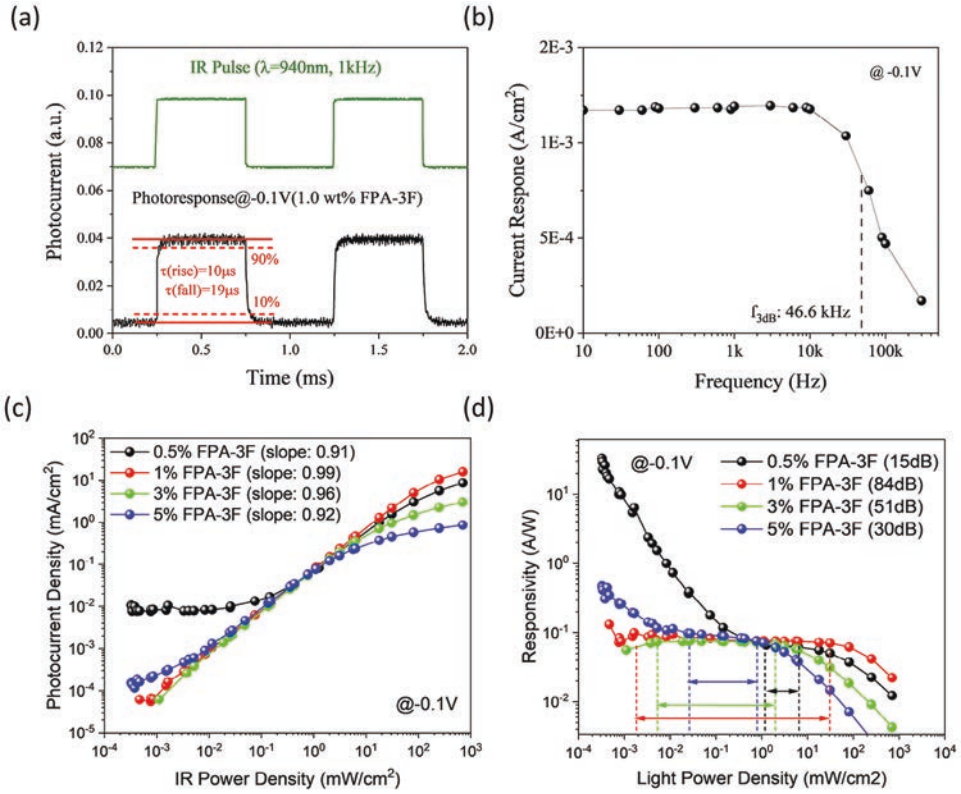

Figure 6. a) Dynamic photocurrent response of organic NIR photodetector with a cross-linked poly-TPD (1.0 wt% FPA-3F) under 940 nm IR perturbation at 1 kHz and b) frequency dependence of the photocurrent signal revealing −3 dB bandwidth of 46.6 kHz, c) linear dynamic range (LDR) of device with different FPA-3F wt% under 940 nm IR illumination and d) corresponding responsivity versus IR power density revealing precise LDR region. The device with 1% FPA-3F shows the highest slope toward 1 along with the widest LDR region of 84 dB.

with chloroform and poured into an excess of H_2O. After separation of the organic layer, the aqueous layer was extracted with chloroform twice. Organic layers were again washed with H_2O and dried over anhydrous $MgSO_4$. The chloroform was removed, and the crude product was purified using flash column chromatography on silica with chloroform as the eluant. The resulting solid was recrystallized from chloroform/n-hexane to obtain the desired compound as a white solid (2.4 g, yield 59%). ^{1}H-NMR (400 MHz, $CDCl_3$) δ (ppm): 4.41 (s, 6H), 1.67 (q, J = 7.6 Hz, 2H), 0.99 (t, J = 7.6 Hz, 3H). ^{13}C-NMR (125 MHz, $CDCl_3$) δ (ppm): 159.05 (s), 146.81 (d, J = 12.6 Hz), 144.95–144.62 (m), 141.68 (d, J = 18.3 Hz), 139.68 (d, J = 17.6 Hz), 124.20 (t, J = 11.9 Hz), 106.93 (t, J = 14.7 Hz), 65.62 (s), 41.15 (s), 22.92 (s), 7.37 (s). ^{19}F-NMR (470 MHz, $CDCl_3$, AA′XX′) δ (ppm): −138.18 to −138.32 (m), −150.45 to −150.59 (m). UV–Vis λ_{max} (in MC) = 267 nm, λ_{max} (spin-coated film) = 272 nm. FT-IR 2130, 1739, 1647, 1483, 1256, 1009 cm^{-1}.

Preparation of Poly-TPD Solution with FPA-3F: Poly-TPD solution and FPA-3F solution of a 10 mg mL^{-1} are prepared in CB. FPA-3F solution was added in poly-TPD solution for the concentration of 0, 0.5, 1, and 3 wt%. All solutions were prepared right before spin-coating.

Preparation of Cross-Linked Poly-TPD Films: Cross-linked poly-TPD films are formed by deep UV irradiation of a peak emission wavelength of 254 nm. 10 mg mL^{-1} poly-TPD (American Dye Source) precursor solutions without or with FPA-3F (0.5, 1, and 3 wt%) in CB are first spin-coated at 4000 rpm for 60 s and annealed at 80 °C for 10 min. The spin-coated poly-TPD films are then cross-linked by UV irradiation with various exposure doses of 50, 100, and 200 mJ cm^{-2} under blowing nitrogen gas condition.

Optical Absorption Spectra Measurement of Cross-Linked Poly-TPD Films before and after Solvent Washing: The optical absorption spectra of the cross-linked poly-TPD films before solvent washing were measured right after the cross-linking process. After the optical absorption measurements, all cross-linked films were spin-coated by CB for solvent washing test. And then, the optical absorption spectra of the cross-linked films after solvent washing were measured.

Preparation of Precursor Solution for NIR Photoactive Layer: The ternary blend polymer photoactive layer was prepared by dissolving PTB7-Th (1-Materials), COi8DFIC (1-Materials), and $PC_{71}BM$ (Nano-C) with a 1:1.05:0.4 weight ratio in CB (Sigma Aldrich). Various concentrations of 13.5, 18, 22.5, 25, 27, and 30 mg mL^{-1} were used for the polymer photoactive layer with various film thicknesses of 90, 120, 150, 167, 180, and 200 nm, respectively. 1,8-Diiodooctane (DIO) (Sigma Aldrich) (1 v/v%) was added to the precursor solution 2 h before spin-coating.

Device Fabrication: Prepatterned indium tin oxide (ITO) coated glass substrates were cleaned with isopropyl alcohol in an ultrasonic cleaner for 30 min. A 10 mg mL^{-1} poly-TPD (American Dye Source) precursor solutions without or with FPA-3F (0.5, 1, and 3 wt%) in CB were spin-coated at 4000 rpm for 60 s and annealed at 80 °C for 10 min. The spin-coated poly-TPD films were cross-linked by UV irradiation with various exposure doses of 50, 100, and 200 mJ cm^{-2} under blowing nitrogen gas condition. The ternary blend polymer precursor solution with various concentrations of 13.5, 18, 22.5, 25, 27, and 30 mg mL^{-1} in CB were spin coated at 2000 rpm for 60 s and annealed at 80 °C for 10 min. The coated substrates were then transferred into the vacuum thermal evaporation chamber. Pressure inside the chamber was then reduced to below 10^{-6} Torr. 10 nm of BCP was deposited followed by 100 nm of Ag. The devices were removed from the vacuum thermal evaporation chamber and encapsulated to prevent exposure to oxygen and moisture during measurement.

Device Characterization: The J–V characterization and the EQE measurement of the photodetectors were conducted using an in-house setup,

© 2024 Wiley-VCH GmbH

16163028, 0, Downloaded from https://onlinelibrary.wiley.com/doi/10.1002/adfm.202403094 by Oklahoma State University, Wiley Online Library on [29/08/2024]. See the Terms and Conditions (https://onlinelibrary.wiley.com/terms-and-conditions) on Wiley Online Library for rules of use; OA articles are governed by the applicable Creative Commons License

the McScience K3100 test system, consisting of a Keithley 2400 source meter, calibrated Si and InGaA photodiodes, a enon DC arc lamp, a monochromator, a current amplifier, a chopper, and a lock-in amplifier. The photoresponse as function of the perturbation frequency was measured by applying a pulsed laser and measured the photocurrent of the device using SR830 lock-in amplifier. The frequency of the pulsed laser can be controlled by a function generator where the frequency is referenced to the lock-in amplifier. The noise spectra of the photodetectors were measured using a Stanford Research SR830 lock-in amplifier coupled with a SR570 low-noise preamplifier.[19] During the measurements, the lock-in frequency of the noise current was set to 1 kHz at −0.1 V bias. Further details of the experimental setup and measurement can be found in the paper by Lee et al.[49]

Supporting Information

Supporting Information is available from the Wiley Online Library or from the author.

Acknowledgements

The authors gratefully acknowledge financial support for the research from the National Science Foundation (NSF) (Award number: 2314294). This research was also supported by the National Aeronautics and Space Administration (NASA) under Agreement No. 80NSSC23M0073. This work was supported by the Technology Innovation Program funded by the Ministry of Trade, Industry and Energy (MOTIE, Korea) [RS-2023-00269383]. This study was supported by Korea Research Institute of Chemical Technology (KRICT) (KS2441-10). This research was also supported by Basic Science Research Program through the National Research Foundation of Korea (NRF) funded by the Ministry of Education (2018R1A6A1A03023788). This work was also supported by grand challenge (GC) program in Korea Institute of Science and Technology. [Correction added on June 25, 2024, after first online publication: The Acknowledgment has been updated in this version.]

Conflict of Interest

The authors declare no conflict of interest.

Data Availability Statement

The data that support the findings of this study are available on request from the corresponding author. The data are not publicly available due to privacy or ethical restrictions.

Keywords

cross-linking, detectivity, electron blocking layer, near-infrared, organic photodetector

Received: February 20, 2024
Revised: June 2, 2024
Published online:

[1] Z. Wang, Y. Gao, Y. Li, H. Yan, F. Kang, Y. Shen, Z.-P. Zhang, G. Wei, H. Fu, *Adv. Funct. Mater.* **2024**, *34*, 2310911.
[2] C. Li, H. Wang, F. Wang, T. Li, M. Xu, H. Wang, Z. Wang, X. Zhan, W. Hu, L. Shen, *Light: Sci. Appl.* **2020**, *9*, 31.
[3] Z. Lan, F. Zhu, *ACS Nano* **2021**, *15*, 13674.
[4] Z. Zhao, C. Xu, L. Niu, X. Zhang, F. Zhang, *Laser Photonics Rev.* **2020**, *14*, 2000262.
[5] T. Zhao, K. Xia, D. Natali, V. Pecunia, *Adv. Opt. Mater.* **2022**, *10*, 2200862.
[6] Y. Wang, Y. Liu, S. Cao, J. Wang, *J. Mater. Chem. C* **2021**, *9*, 5302.
[7] C. Li, W. Huang, L. Gao, H. Wang, L. Hu, T. Chen, H. Zhang, *Nanoscale* **2020**, *12*, 2201.
[8] J. R. Manders, T.-H. Lai, Y. An, W. Xu, J. Lee, D. Y. Kim, G. Bosman, F. So, *Adv. Funct. Mater.* **2014**, *24*, 7205.
[9] M. A. Green, *Nat. Energy* **2016**, *1*, 15015.
[10] A. C. Arias, J. D. Mackenzie, I. McCulloch, J. Rivnay, A. Salleo, *Chem. Rev.* **2010**, *110*, 3.
[11] J. Lee, S.-J. Ko, H. Lee, J. Huang, Z. Zhu, M. Seifrid, J. Vollbrecht, V. V. Brus, A. Karki, H. Wang, K. Cho, T.-Q. Nguyen, G. C. Bazan, *ACS Energy Lett.* **2019**, *4*, 1401.
[12] J. Huang, J. Lee, J. Vollbrecht, V. V. Brus, A. L. Dixon, D. X. Cao, Z. Zhu, Z. Du, H. Wang, K. Cho, G. C. Bazan, T.-Q. Nguyen, *Adv. Mater.* **2020**, *32*, 1906027.
[13] Z. Xiao, X. Jia, L. Ding, *Sci. Bull.* **2017**, *62*, 1562.
[14] H. Li, Z. Xiao, L. Ding, J. Wang, *Sci. Bull.* **2018**, *63*, 340.
[15] W. Li, Y. Xu, X. Meng, Z. Xiao, R. Li, L. Jiang, L. Cui, M. Zheng, C. Liu, L. Ding, Q. Lin, *Adv. Funct. Mater.* **2019**, *28*, 1808948.
[16] C. Chan, T. Liu, J. Zhou, Y. He, D. Luo, Z. Jiang, Z. Wang, Q. Liu, C. Li, F. Zhang, E. Zhou, K. Wang, A. K. K. Kyaw, *Chem. Eng. J.* **2023**, *471*, 144451.
[17] G. Simone, M. J. Dyson, S. C. J. Meskers, R. A. Janssen, G. H. Gelinck, *Adv. Funct. Mater.* **2020**, *30*, 1904205.
[18] J. Huang, J. Lee, H. Nakayama, M. Schrock, D. Cao, K. Cho, G. C. Bazan, T.-Q. Nguyen, *ACS Nano* **2021**, *15*, 1753.
[19] J. Kublitski, A. Hofacker, B. K. Boroujeni, J. Benduhn, V. C. Nikolis, C. Kaiser, D. Spoltore, H. Kleemann, A. Fischer, F. Ellinger, K. Vandewal, K. Leo, *Nat. Commun.* **2021**, *12*, 551.
[20] G. Konstantatos, I. Howard, A. Fisher, S. Hoogland, J. Clifford, E. Klem, L. Levina, E. H. Sargent, *Nature* **2006**, *442*, 180.
[21] R. Comparelli, F. Zezza, M. Striccoli, M. L. Curri, R. Tommasi, A. Agostiano, *Mater. Sci. Eng. C* **2003**, *23*, 1083.
[22] K. M. Noone, N. C. Anderson, N. E. Horwitz, A. M. Munro, A. P. Kulkarni, D. S. Ginger, *ACS Nano* **2009**, *3*, 1345.
[23] G. Saraqueta, K. R. Choundhury, J. Subbiah, F. So, *Adv. Funct. Mater.* **2011**, *21*, 167.
[24] X. Wang, J. Huang, J. Li, J. Yu, *J. Phys. D: Appl. Phys.* **2016**, *49*, 075102.
[25] X. Wang, L. Lv, L. Li, Y. Chen, K. Zhang, H. Chen, H. Dong, J. Huang, G. Shen, Z. Yang, H. Huang, *Adv. Funct. Mater.* **2016**, *26*, 6306.
[26] T. Zhang, L. C. Winkler, J. Wolansky, J. Schröder, K. Leo, J. Benduhn, *Adv. Funct. Mater.* **2024**, *34*, 2308719.
[27] V. Yeddu, G. Seo, F. Cruciani, P. M. Beaujuge, D. Y. Kim, *ACS Photonics* **2019**, *6*, 2368.
[28] P. E. Keivanidis, P. K. H. Ho, R. H. Friend, N. C. Greenham, *Adv. Funct. Mater.* **2010**, *20*, 3895.
[29] J. Wang, Q. Zheng, *J. Mater. Chem. C* **2019**, *7*, 1544.
[30] Z. Zhong, F. Peng, Z. Huang, L. Ying, G. Yu, F. Huang, Y. Cao, *ACS Appl. Mater. Interfaces* **2020**, *12*, 45092.
[31] M. P. Jong, L. J. Ijzendoorn, M. J. Voigt, *Appl. Phys. Lett.* **2000**, *77*, 2255.
[32] J.-S. Kim, R. H. Friend, I. Grizzi, J. H. Burroughes, *Appl. Phys. Lett.* **2005**, *87*, 023506.
[33] T. N. Le, H. Kim, R. Elumalai, J. Kim, J. Lee, M. C. Suh, *Chem. Eng. J.* **2023**, *471*, 144540.

© 2024 Wiley-VCH GmbH

16163028, 0, Downloaded from https://onlinelibrary.wiley.com/doi/10.1002/adfm.202403094 by Oklahoma State University, Wiley Online Library on [29/08/2024]. See the Terms and Conditions (https://onlinelibrary.wiley.com/terms-and-conditions) on Wiley Online Library for rules of use; OA articles are governed by the applicable Creative Commons License

[34] S. L. Kwak, H. J. Park, J.-H. Jang, J. Y. Park, J. M. Park, J. Lee, D. H. Hwang, *Chem. Eng. J.* **2023**, *454*, 139944.
[35] W. Feng, Z. Lin, J. Cui, W. Lv, W. Wang, Q. Ling, *Sol. Energy Mater. Sol. Cells* **2019**, *200*, 109982.
[36] M. Casutt, M. Ruscello, N. Strobel, S. Koser, U. H. F. Bunz, D. Jänsch, J. Freudenberg, G. Hernandez-Sosa, K. Müllen, *Chem. Mater.* **2019**, *31*, 7657.
[37] K. Kim, S. Shin, S. H. Kim, J. Lee, T. K. An, *Appl. Surf. Sci.* **2019**, *479*, 280.
[38] H. Kwon, X. Tang, S. Shin, J. Hong, W. Jeong, Y. Jo, T. K. An, J. Lee, S. H. Kim, *ACS Appl. Mater. Interfaces* **2020**, *12*, 30600.
[39] Q. Sun, G. Subramanyam, L. Dai, M. Check, A. Campbell, R. Naik, J. Grote, Y. Wang, *ACS Nano* **2009**, *3*, 737.
[40] B. W. H. Saes, M. M. Wienk, R. A. J. Janssen, *RSC Adv.* **2020**, *10*, 30176.
[41] X. Zhao, Z.-K. Tan, *Nat. Photonics* **2020**, *14*, 215.
[42] B. Liu, R.-Q. Png, L.-H. Zhao, L.-L. Chua, R. H. Friend, P. H. K. Ho, *Nat. Commun.* **2012**, *3*, 1321.
[43] N. Cho, H.-L. Yip, J. A. Davies, P. D. Kazarinoff, D. F. Zeigler, M. M. Durban, Y. Segawa, K. M. O'Malley, C. K. Luscombe, A. K.-J. Jen, *Adv. Energy Mater.* **2011**, *1*, 1148.
[44] Y. Zou, Y. Liu, M. Ban, Q. Huang, T. Sun, Q. Zhang, T. Song, B. Sun, *Nanoscale Horiz.* **2017**, *2*, 156.
[45] C. Tao, M. Aljada, P. E. Shaw, K. H. Lee, H. Cavaye, M. N. Balfour, R. J. Borthwick, M. James, P. L. Burn, I. R. Gentle, P. Meredith, *Adv. Energy Mater.* **2013**, *3*, 105.
[46] S. L. Kwak, H. J. Park, J. Jang, J. Y. Park, J. M. Park, J. Lee, D. Hwang, *Chem. Eng. J.* **2023**, *454*, 139944.
[47] J. Y. Park, S. L. Kwak, H. J. Park, D. Hwang, *Nanomaterials* **2023**, *13*, 1934.
[48] J. Y. Park, J. Jang, J. Lee, D. Hwang, *J. Nanosci. Nanotechnol.* **2020**, *20*, 4661.
[49] M. J. Kim, M. Lee, H. Min, S. Kim, J. Yang, H. Kweon, W. Lee, D. H. Kim, J.-H. Choi, D. Y. Ryu, M. S. Kang, B. S. Kim, J. H. Cho, *Nat. Commun.* **2020**, *11*, 1520.
[50] H. M. Haverinen, R. A. Myllylä, G. E. Jabbour, *Appl. Phys. Lett.* **2009**, *94*, 073108.
[51] X. Zhou, D. Yang, D. Ma, *Adv. Opt. Mater.* **2015**, *3*, 1570.
[52] M. C. Weidman, M. E. Beck, R. S. Hoffman, F. Prins, W. A. Tisdale, *ACS Nano* **2014**, *8*, 6363.
[53] J. W. Lee, D. Y. Kim, S. Baek, H. Yu, F. So, *Small* **2016**, *12*, 1328.
[54] X. Gong, M. Tong, Y. Xia, W. Cai, J. S. Moon, Y. Cao, G. Yu, C.-L. Shieh, B. Nilsson, A. J. Heeger, *Science* **2009**, *325*, 1665.

© 2024 Wiley-VCH GmbH

16163028, 0, Downloaded from https://onlinelibrary.wiley.com/doi/10.1002/adfm.202403094 by Oklahoma State University, Wiley Online Library on [29/08/2024]. See the Terms and Conditions (https://onlinelibrary.wiley.com/terms-and-conditions) on Wiley Online Library for rules of use; OA articles are governed by the applicable Creative Commons License